*Korean J. Chem. Eng.*, 33(1), 330-336 (2016)
DOI: 10.1007/s11814-015-0142-7

pISSN: 0256-1115
eISSN: 1975-7220

# Morphology, thermal, mechanical, and barrier properties of graphene oxide/poly(lactic acid) nanocomposite films

**Seong Woo Kim† and Hyun Muk Choi**

Department of Chemical Engineering, Kyonggi University,
154-42, Gwanggyosan-ro, Yeongtong-gu, Suwon, Gyeonggi-do 16227, Korea
(*Received 26 February 2015 • accepted 29 June 2015*)

**Abstract**−To improve the physical and gas barrier properties of biodegradable poly(lactic acid) (PLA) film, two graphene nanosheets of highly functionalized graphene oxide (0.3 wt% to 0.7 wt%) and low-functionalized graphene oxide (0.5 wt%) were incorporated into PLA resin via solution blending method. Subsequently, we investigated the effects of material parameters such as loading level and degree of functionalization for the graphene nanosheets on the morphology and properties of the resultant nanocomposites. The highly functionalized graphene oxide (GO) caused more exfoliation and homogeneous dispersion in PLA matrix as well as more sustainable suspensions in THF, compared to low-functionalized graphene oxide (LFGO). When loaded with GO from 0.3 wt% to 0.7 wt%, the glass transition temperature, degree of crystallinity, tensile strength and modulus increased steadily. The GO gave rise to more pronounced effect in the thermal and mechanical reinforcement, relative to LFGO. In addition, the preparation of fairly transparent PLA-based nanocomposite film with noticeably improved barrier performance achieved only when incorporated with GO up to 0.7 wt%. As a result, GO may be more compatible with hydrophilic PLA resin, compared to LFGO, resulting in more prominent enhancement of nanocomposites properties.

Keywords: Graphene Oxide, Poly(Lactic Acid), Nanocomposite Film, Barrier Properties

## INTRODUCTION

In recent decades, requirement for the use of ecologically safe biodegradable polymers for short-term packaging and disposable items has consistently been increasing since undegradable synthetic polymer wastes can cause a serious global environmental problem [1,2]. To replace traditional undegradable polymers, accordingly, various biodegradable polymers, such as aliphatic polyester including poly(lactic acid) (PLA), poly($\varepsilon$-caprolactone) (PCL), poly(butylene succinate) (PBS), poly(ethylene succinate) (PES), and poly(hydroxyl butyrate) (PHB), have been developed and industrialized [3]. Among these, PLA has been of great interest due to its renewable resources, biodegradability, biocompatibility, good mechanical properties, fabricability, and competitive cost, thus being a promising polymer for diverse end-use applications [4-6].

Although the biodegradable PLA resin has a number of advantages, it still shows a limitation in the application of gas barrier packaging films due to its inferior mechanical properties and poor gas permeation resistance compared to conventional petrochemical-based polymers. Therefore, considerable efforts have been made to improve the properties of PLA resins by combining them with inorganic species. These attempts have been performed by the incorporation of organically modified clay platelets [7,8] or inorganic silica particles [9,10] with nanoscale dimensions into PLA matrix to produce biodegradable nanocomposite with improved properties. Owing to restricted aspect ratios of the nanoclay platelets and silica particles, however, a fairly larger amount of inorganic materials should be incorporated to increase the performance to the level required in high barrier packaging films.

Recently, graphene nanosheet, a single layer of graphite, has gained tremendous attention in the field of polymer-based nanocomposites due to its great potential for enhancing mechanical, electrical, thermal, and gas barrier properties of host polymers [11]. In particular, this nanofiller with atomically thin, distinctive planar structure is a promising candidate for the application of gas barrier packaging films, due to its gas-impermeable characteristic and very high aspect ratio, which makes high barrier nanocomposites possible at extremely small loading by effectively increasing tortuous paths for gas molecule permeation. A variety of graphene nanosheets such as expanded pristine graphite [12,13], functionalized or modified graphene oxide [14-16], and thermally or chemically reduced graphene [17,18], have been utilized to prepare the polymer-based nanocomposites with improved properties. It has been reported that the improvement in the gas barrier and mechanical properties of the PLA polymer could be achieved by incorporating two different types of graphene nanosheets including GO and expanded unfunctionalized graphene nanoplatelets [19]. In addition, the influence of graphene nanosheets loading on the crystallization behavior of PLA has also been studied [20-22].

In the present work, we prepared biodegradable PLA-based nanocomposite films with enhanced properties by employing two different exfoliated graphene oxide nanosheets with high and low levels of chemical functionalization on their surfaces. We also explored the effects of the level of graphene nanosheets loading and degree

†To whom correspondence should be addressed.
E-mail: wookim@kyonggi.ac.kr

of functionalization of graphene oxide on the morphology, optical, thermal, mechanical and gas barrier properties of the prepared nanocomposite films in terms of measurement of visible light transmittance, glass transition and thermal degradation temperatures, tensile properties, and oxygen transmission rate (OTR).

## EXPERIMENTAL

### 1. Materials

Poly(lactic acid) resin (PLA, 4032D, Natureworks Co. Ltd.) was used as an organic polymer matrix in the graphene/PLA nanocomposites. Natural graphite powders with an average particle size of 140 μm were obtained from Sigma-Aldrich. As the oxidants for oxidizing the graphite, potassium disulfate ($K_2O_8S_2$, 99.0%), phosphorous pentoxide ($P_2O_5$, 99.0%), and potassium permanganate ($KMnO_4$, 99.0%) were also purchased from Sigma-Aldrich. Concentrated sulfuric acid ($H_2SO_4$, 95%), hydrogen peroxide ($H_2O_2$, 34.5%), tetrahydrofuran (THF, 99.5 %), and hydrochloride (HCl, 35%) were purchased from Duksan Chemical, and deionized (DI) water was used throughout the experiments. The materials were used as received without further purification.

The exfoliated graphene oxide (GO) nanosheets were prepared from natural graphites via oxidation process based on modified Hummer's method [23] followed by sonication. The detailed experimental procedures for the preparation of graphene oxide are illustrated elsewhere [24]. The graphene oxide with a small number of oxygen-containing functional groups on its surface was also prepared by using mild oxidation conditions such as the amount of $KMnO_4$ and reaction time, which was designated as LFGO. Table 1 shows the oxidation conditions used for the preparation of two different graphene oxides, GO and LFGO, and their atomic composition measured from elemental analysis.

### 2. Preparation of Nanocomposite Films

The transparent GO/PLA nanocomposite thin films with a thickness of ca. 40 μm were prepared via solution-processed blending and casting method. PLA resin with a pellet form was dissolved in a THF solvent through magnetic stirring at 60 °C to obtain homogeneous PLA solution, and then a given amount of GO suspension in water was added into the PLA solution with vigorous stirring for 30 min. Subsequently, the GO/PLA solution was subjected to sonication for 15 min to derive the exfoliation of residual stacked or intercalated graphite. The resulting GO/PLA solution with a homogeneous dispersion was deposited followed by casting on a glass substrate using a micrometer film applicator (1117, SI Co.). The cast films were then dried at 60 °C for 20 min in a vacuum dryer (VH-PO-64, Lab. House Co.). After drying process, the GO/PLA thin film was carefully detached from the glass substrate. The incorporated GO content in the nanocomposite samples was varied at 0.3, 0.5, 0.7 wt%, but the LFGO content was fixed at 0.5 wt%. All of the dried samples were kept in a dessicator to prevent the moisture influence prior to performing characterization.

**Table 1. Oxidation conditions for the preparation of GO and LFGO, and their atomic composition obtained from elemental analysis**

| Sample | Oxidation condition | | Elemental analysis | | |
|---|---|---|---|---|---|
| | Reaction time (min) | Amount of $KMnO_4$ (g) | C (%) | H (%) | O (%) |
| GO | 120 | 6 | 53.5 | 1.7 | 43.6 |
| LFGO | 60 | 2 | 71.5 | 1.2 | 27.2 |

### 3. Characterization

The atomic concentrations for the GO and LFGO were measured by elemental analyzer (Flash EA1112, Thermo). X-ray diffractometer (D8-Discover, Bruker Co.) was used to analyze the interlayer spacing of GO as synthesized and the extent of exfoliation for the GO as dispersed in PLA matrix. The Cu K$\alpha$ radiation source was operated at 40 kV and 150 mA. The scanning rate was 1.0°/min in the range of 5-40°. The nanofillers such as graphite, GO, and LFGO were analyzed in the form of powder, while GO/PLA nanocomposite was analyzed as a film. The morphologies of GO/PLA nanocomposites were observed using a transmission electron microscope (TEM, JEM-2100F, JEOL, Japan) operated at 200 kV of accelerating voltage. The samples for TEM images were prepared in the form of thin film with a thickness less than 100 nm using ultramicrotome equipped with a diamond knife. Differential scanning calorimetry (DSC7020, Seico, Japan) was used to examine the variance of thermal properties including glass transition temperature ($T_g$) and melting temperature ($T_m$) of the nanocomposites as a function of graphene oxide loading. The heating thermogram was obtained by heating the samples from room temperature to 200 °C at a heating rate of 10 °C/min under nitrogen gas flow. The thermal stability was also examined by using an Exstar 6000 (TG/DTA6100, Seiko, Japan) thermogravimetric analyzer. The sample was heated from room temperature to 700 °C at a heating rate of 10 °C/min under nitrogen gas flow. The optical transparency of the prepared GO/PLA nanocomposite film was measured with a visible spectrophotometer (Optizen 1412V, Mecasys Co., Korea) in the visible-light wavelength range of 400 nm-800 nm. Tensile properties of the nanocomposite films were measured by using a universal testing machine (QM100S, Qmesys, Korea) operating at 20 mm/min of cross-head speed. Nine samples with dimensions of 15 mm (width)×100 mm (length) were tested and an average value was taken. The oxygen transmission rate (OTR) of the nanocomposite film was measured according to ASTM D 3985 using an OX-TRAN 2/10 (Mocon Inc., USA). The oxygen permeation tests were performed at 23 °C and 0% relative humidity.

## RESULTS AND DISCUSSION

### 1. Morphological Characterization of Graphene Oxide in the Nanocomposites

It has been recognized that homogeneous dispersion of nanofillers in the polymer matrix coupled with their highly exfoliated or intercalated structure is the most essential parameter for the preparation of polymer-based nanocomposites with improved thermal, mechanical, and gas barrier properties. In this study, the morphologies of prepared graphene/PLA nanocomposites were examined by both XRD analysis and TEM observation. Fig. 1 displays the measured XRD patterns in the 2$\theta$ range of 5-40° for (a) pristine graphite, synthesized two different graphene oxide nanosheets, and

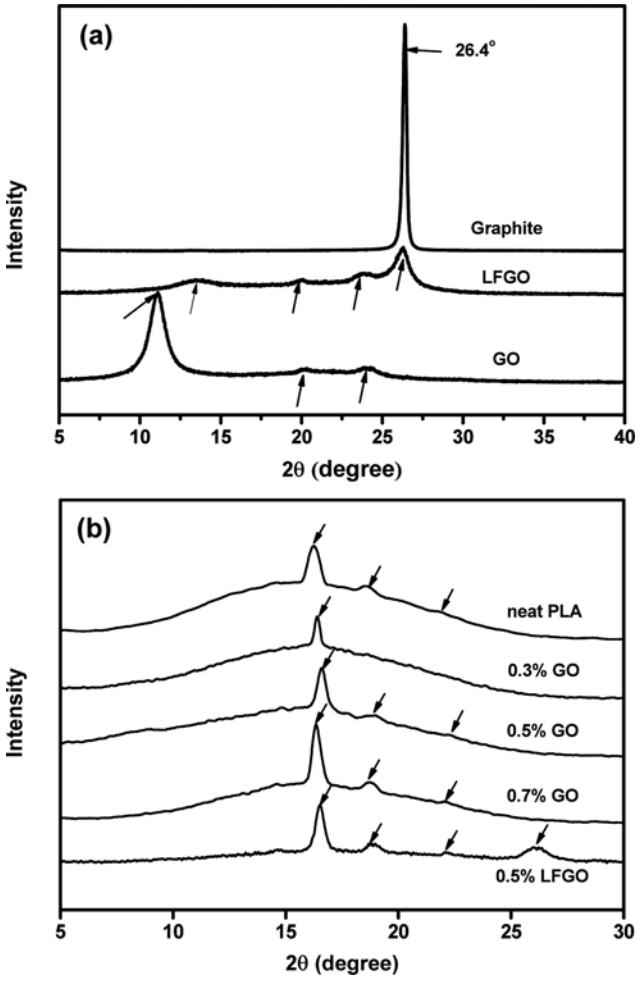


**Fig. 1. XRD patterns for the (a) pristine graphite, GO, and LFGO, and (b) neat PLA, corresponding nanocomposites with various GO loading and 0.5 wt% LFGO.**

(b) neat PLA and corresponding nanocomposite films. Variations of layer-to-layer distance in stacked graphene nanosheets after functionalization could be quantitatively determined from X-ray diffraction. In the XRD pattern of natural graphite, the characteristic sharp diffraction peak was observed at $2\theta$=26.4°, which originates from the graphene interlayer spacing ($d_{002}$=0.34 nm). The functionalized graphene oxide sample (GO) showed an XRD pattern where the diffraction peak was shifted to a lower angle at $2\theta$=11.1°, corresponding to an interlayer distance of 0.80 nm, and furthermore peak broadening occurred due to the disorder caused by diminished crystalline size [17]. On the other hand, the low-functionalized graphene oxide (LFGO) showed a different XRD pattern with a decreased characteristic peak at its original $2\theta$ location, implying that the LFGO partially maintained the original status of pristine graphite because of incomplete intercalation due to lack of functional groups introduced onto graphite surface. In Fig. 1(b) showing the XRD patterns of GO/PLA nanocomposite films with various GO contents, an obvious disappearance of the GO characteristic peak at $2\theta$=11.1° could be detected, while only PLA characteristic peaks at $2\theta$=16.3°, 19.1°, and 22.4° were observed, indicating the complete exfoliation of graphite particles into individual graphene nanosheets or the layer disorder resulting from loss of graphene structure regularity [25]. In the case of 0.5% LFGO-filled nanocomposite, however, the original characteristic peak of pristine graphite remained at $2\theta$=26.4°, despite diffusion and penetration of PLA chain molecules into graphene interlayer spacing during solution blending. This suggests that the domains consisting of densely stacked layers like original graphite status exist in the LFGO/PLA nanocomposite sample, along with partially intercalated or exfoliated graphene nanosheets.

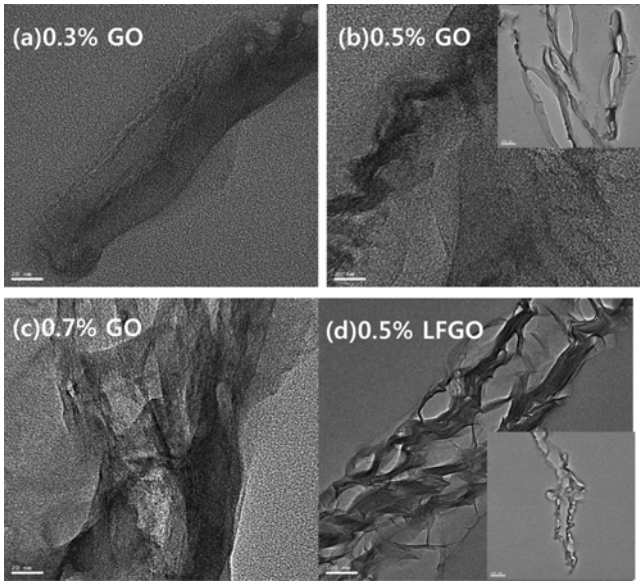


**Fig. 2. TEM images of PLA nanocomposites containing 0.3, 0.5, 0.7 wt% GO and 0.5 wt% LFGO.**

TEM images of the ultramicrotomed cross-sections of the nanocomposites are shown in Fig. 2. The images for the GO-incorporated nanocomposites demonstrated highly intercalated or fully exfoliated GO nanosheets randomly dispersed in the PLA matrix, while there were some tactoid-like domains with a few restacks together. Moreover, when graphene loading increased, the incorporated graphene nanosheets were observed to be more crumpled, and the number of stacked layers increased. In the case of LFGO-incorporated nanocomposite, however, many thick agglomerates with more closely graphene layers were distributed through the PLA matrix. Moreover, from the 200 nm-scale images (inset) in the figure (b) and (d), it could be seen that graphene sheets with few layer were oriented in the parallel direction to the plane of nanocomposite film, which may have been caused by shear flow during solution casting process.

Based on TEM observation and XRD result, it was confirmed that the degree of functionality on the graphite was strongly associated with the nanostructured morphology such as intercalated or exfoliated structure in the graphene-incorporated nanocomposites. For the hydrophilic PLA resin used in this study, highly functionalized graphite gave rise to more exfoliated graphene nanosheets homogeneously dispersed in the polymer matrix, compared to low-functionalized graphite, which may be attributed to preferential formation of strong interaction between graphene surface and PLA molecules.

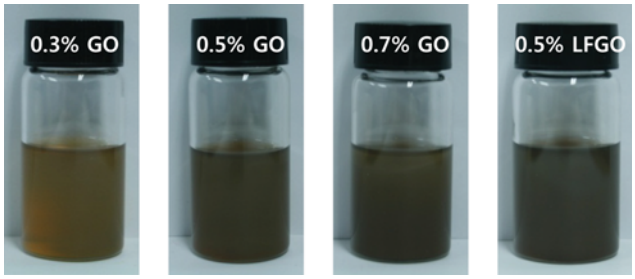


**Fig. 3. Digital images of GO and LFGO-incorporated PLA nanocomposite suspensions in THF solvent.**

Fig. 3 shows digital photographs of graphene oxide-filled PLA nanocomposite suspensions in THF solvent. Initially, both of GO and LFGO were observed to be uniformly dispersed in PLA solution. However, LFGO-dispersed suspension showed a layer of sediment deposited on the bottom of glass bottle within 1 day, which may have originated from a weak interaction between PLA molecule and graphene oxide nanosheet, while the GO suspension maintained a homogeneous dispersion for more than three days, irrespective of nanofiller content. Additionally, when GO was added with load of 0.3 wt% and 0.5 wt%, the dispersions were yellowish brown and dark brown color, respectively, as shown in the figure, whereas the suspensions containing LFGO exhibited a deep black color, probably due to the maintenance of the original $\pi$-conjugation system for the LFGO with low polar functionality on the surface [26,27].

**2. Thermal Properties**

In the semi-crystalline polymer-based nanocomposites, the degree of crystallinity and the crystalline structure induced from the crystallization process under presence of nanofillers generally affect the performance of the final nanocomposites, in addition to reinforcing effect of nanofiller itself. In this study, hence, the effect of incorporated graphene nanosheets on the thermal behavior of the PLA polymer was investigated through DSC experiment.

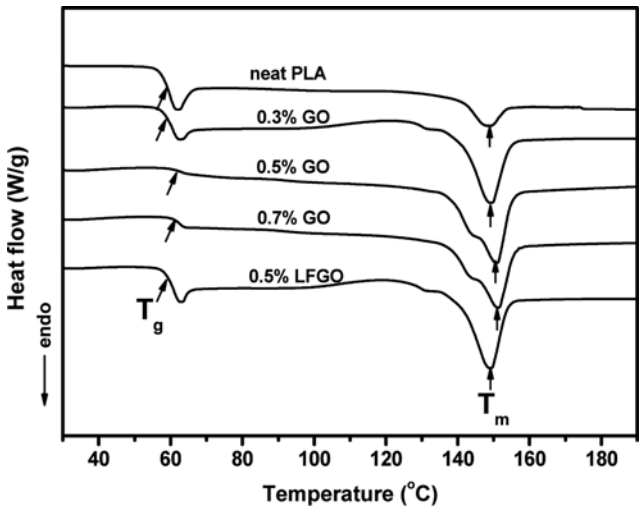


**Fig. 4. DSC heating thermograms of neat PLA and corresponding nanocomposites with various loading of GO and 0.5 wt% LFGO.**

**Table 2. Thermal properties of neat PLA and nanocomposites incorporated with GO and LFGO**

| Sample | DSC result | | | | TGA result | |
|---|---|---|---|---|---|---|
| | $T_g$ (°C) | $T_m$ (°C) | $\Delta H_f$ (J/g) | $\chi_c$ (%) | $T_2$ (°C) | $T_{50}$ (°C) |
| Neat PLA | 57.5 | 148.8 | 9.1 | 9.7 | 309.8 | 353.8 |
| 0.3% GO | 60.4 | 149.1 | 23.3 | 25.0 | - | - |
| 0.5% GO | 62.8 | 150.6 | 30.8 | 33.1 | 301.3 | 352.4 |
| 0.7% GO | 63.0 | 151.0 | 29.7 | 32.0 | - | - |
| 0.5% LFGO | 60.7 | 149.0 | 29.2 | 31.4 | 311.8 | 359.9 |

Fig. 4 shows DSC heating thermograms of neat PLA and its nanocomposites with various GO content and 0.5 wt% LFGO. Neat PLA sample was also prepared in the form of solution-cast film. The thermal properties such as glass transition temperature ($T_g$), melting temperature ($T_m$), heat of fusion ($\Delta H_f$), and degree of crystallinity ($\chi_c$) were determined from these thermograms and summarized in Table 2. The degree of crystallinity of PLA in the nanocomposites was obtained from the following equation:

$$\chi_c(\%) = \frac{\Delta H_f}{\Delta H_{f,PLA}(1-W_f)} \times 100\% \quad (1)$$

where $\Delta H_f$ is the enthalpy of fusion of sample; $\Delta H_{f,PLA}$ refers to the heat of fusion for 100% crystalline PLA, which was set as 93 J/g, and $W_f$ is the mass fraction of nanofiller in the nanocomposite [28]. The addition of graphene nanosheet into the PLA matrix was found to increase the $T_g$ value of PLA in the nanocomposite, regardless of degree of functionalization on the graphene nanosheet surface. Furthermore, increasing the GO loading level resulted in the steady increase in the $T_g$ of the GO/PLA nanocomposite. Such a reinforcing effect in the thermal property may be ascribed to the reduced mobility of PLA chain molecules in the nanocomposites, resulting from the interaction between functionalized graphene oxide surface and hydrophilic PLA molecules [19]. Similar results have also been reported for a number of nanocomposites incorporated with various nanofillers such as nanosilica particles [29,30], nanoclays [31,32], cellulose nanofiber [33], and graphene nanosheets [13,14,19]. It should be noted that the GO led to a more substantial increase in $T_g$ of the nanocomposite, compared to LFGO, because GO could yield more increased interaction between two phases due to larger amount of functional groups on its basal plane.

As regards crystallization behavior, the $\chi_c$ of PLA in the nanocomposite was revealed to remarkably increase by the incorporation of only small amount of graphene nanosheets. It could be seen that the incorporation of GO led to steep increase in $\chi_c$ up to low content of 0.3 wt%, but further loading resulted in only a slight increase. When added with 0.5 wt% GO, the $\chi_c$ increased from 9.7% for the neat PLA to 33.1% for the nanocomposite. The graphene nanosheets incorporated into the PLA matrix may be considered as extraneous nucleating agents promoting the crystallization rate, and thus yielded the noticeable improvement in the degree of crystallinity for PLA in the nanocomposites. Additionally, the GO exhibited a more pronounced effect on the crystallization behavior

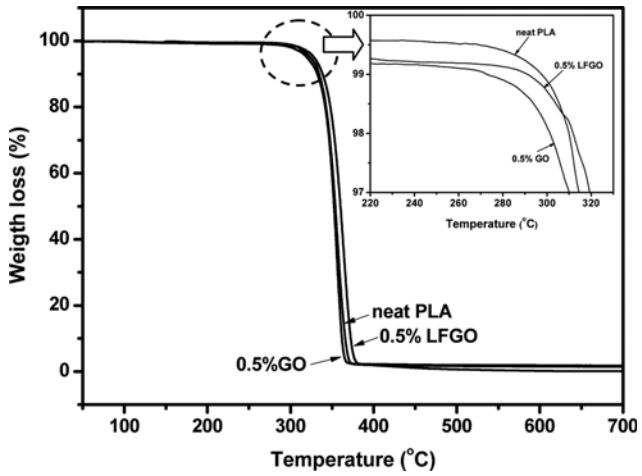


**Fig. 5. TGA thermograms of neat PLA and corresponding nanocomposite containing GO and LFGO at 0.5 wt%.**

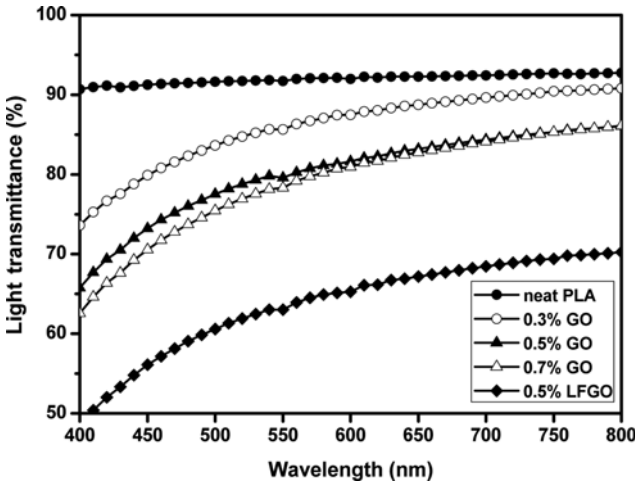


**Fig. 6. Visible light transmittance for the neat PLA film and corresponding nanocomposite films with various GO loading and 0.5 wt% LFGO.**

compared to LFGO, which may be associated with uniform dispersion as well as exfoliated structure of the graphene nanosheets in the PLA matrix. The crystallization process acceleration caused by the incorporation of nanofillers has also been reported for a variety of crystalline polymer-based nanocomposites [12,34,35].

The thermal stability of biodegradable PLA nanocomposite incorporated with small amount of graphene nanosheet was also assessed by thermogravimetric analysis (TGA). Fig. 5 shows TGA thermograms of neat PLA and corresponding nanocomposites with 0.5 wt% of GO and LFGO. As thermal stability parameters, $T_2$ and $T_{50}$, which were defined as degradation temperatures at 2% and 50% weight loss, respectively, were determined from the thermograms and listed in Table 2. Both $T_2$ and $T_5$ of the nanocomposites were reduced with incorporation of GO as compared to those of neat PLA, but when LFGO was incorporated, they were increased with an opposite trend to the GO-incorporated nanocomposite. Consequently, the added GO nanofillers were revealed to deteriorate the thermal stability of the nanocomposite, possibly due to pyrolysis of a number of unstable oxygen-containing functional groups attached onto the surface or edge of the GO platelets [15]. However, the thermal stability was enhanced when incorporated with the LFGO nanofillers containing lower amount of functional groups relative to GO, suggesting that a high degree of functionality on graphene surface could cause high extent of exfoliation as well as good dispersion of the graphene nanosheets, but result in poor thermal stability of resultant nanocomposites due to their surface characteristics.

### 3. Optical Transparency

In the development of biodegradable PLA-based food packaging nanocomposite film with enhanced gas barrier performance, minimizing the reduction of optical transparency, which generally originates from light scattering caused by nanofillers distributed within the film, is of great importance, because transparent film enables consumers to clearly identify the inner food conditions such as freshness or spoilage. Accordingly, to assess the feasibility of the application of graphene-incorporated nanocomposite film prepared in this work to transparent food packaging film, the influence of graphene addition on the optical transparency of the nanocomposite film was investigated. Fig. 6 shows the relative visible light transmittance in the wavelength range of 400 nm-800 nm for the neat PLA and nanocomposite films. As expected, the neat PLA film was observed to be highly transparent, transmitting over 92% of incident visible light over the entire wavelength range. The incorporation of graphene nanosheets was revealed to diminish optical transparency of the nanocomposite film due to the increased light scattering and diffusivity in the film. For instance, two different nanocomposite films containing GO at 0.3 wt% and 0.5 wt% showed light transmittance ranging from 85% to 90% and from 80% to 84% in the visible light region, respectively. This result indicates that incorporation of highly functionalized GO with load of below 0.7 wt% can yield nanocomposite film retaining a fairly good transparency with light transmittance over 80%, leading to utilization as food packaging films. In the case of 0.5 wt% LFGO-incorporated nanocomposite film; however, the light transmittance was severely decreased below 70%, yielding poor transparency, which may be ascribed to the graphite tactoids with tightly stacked layers dispersed in the PLA matrix, responsible for the increased extent of light scattering.

### 4. Mechanical Properties

A tensile deformation test was performed to assess the extent of mechanical reinforcement resulting from the incorporation of graphene nanosheets possessing superior mechanical properties into PLA resin. Fig. 7 shows the measured tensile properties of nanocomposite films as a function of graphene nanosheet loading. As the incorporated GO content increased, the tensile strength at break and tensile modulus of the resultant nanocomposite film were improved. Especially, with only a small amount of GO incorporation at 0.3 wt%, remarkable increase in both tensile properties was observed. As included in the figure, the LFGO-incorporated nanocomposite film exhibited lower tensile strength and modulus, as compared with the film containing GO at the same content, which may stem from the low degree of exfoliation of LFGO as well as poor compatibility between LFGO and PLA phases. In general, the tensile modulus as a measure of stiffness is improved at the expense

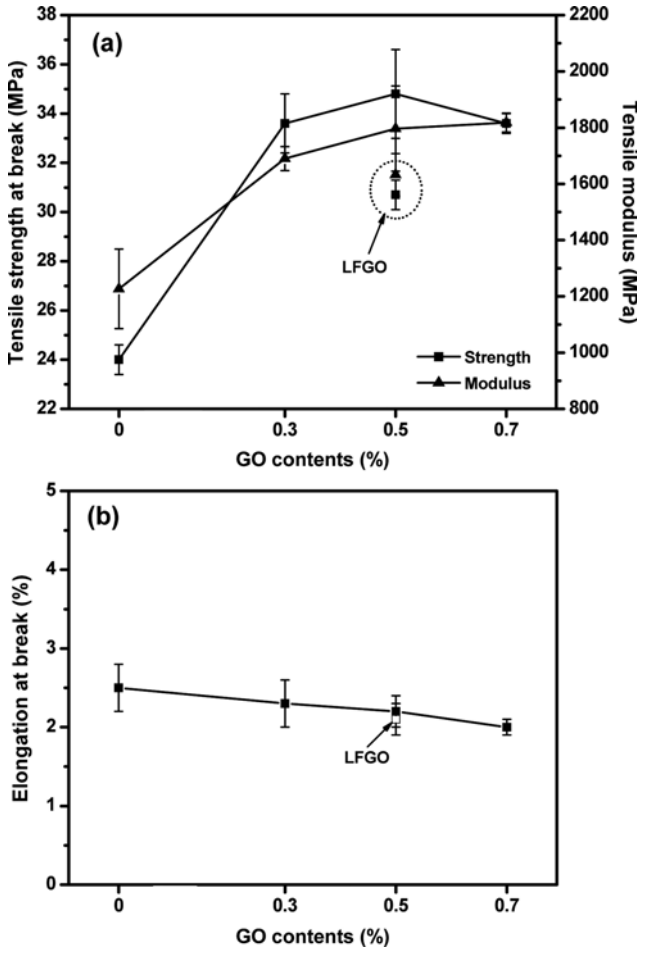


**Fig. 7. Tensile properties of GO/PLA films with various GO loading (0 to 0.7 wt%) and LFGO/PLA film with 0.5 wt% LFGO: (a) tensile strength at break and tensile modulus, (b) elongation at break.**

of elongation representing the degree of ductility when the reinforcing nanofillers are incorporated into polymer matrix. In this study, the incorporation of graphene nanosheet also caused the decrease in elongation at break of the resultant nanocomposite film, but the extent of reduction was revealed to be very slight, which may be attributed to easily deformable nature of graphene imbedded in polymer matrix. For instance, the incorporation of GO at the maximum content of 0.7 wt% reduced the elongation of the nanocomposite film by only 0.49% relative to that of neat PLA film. In addition, the effect of the degree of functionality of the graphene surface on the elongation property was shown to be insignificant. The tensile properties of elongation at break for the nanocomposite films containing GO and LFGO at 0.5 wt% were measured to be 2.18% and 2.15%, respectively, demonstrating almost identical level of ductility. Based on sustainability of elongation property even after the incorporation of graphene nanosheets into PLA resin, it is believed that the nanocomposite films prepared in this study may be utilized for the application of practical packaging film requiring a proper level of ductility.

**5. Barrier Properties**

The influence of graphene nanosheets incorporation on the variation of gas barrier property of the PLA resin was assessed in terms of measurement of oxygen transmission rate (OTR) through the prepared nanocomposite film in the perpendicular direction. Fig. 8 shows the oxygen transmission rate (OTR) for the neat PLA film and the corresponding nanocomposite films with various GO loading from 0.3 wt% to 0.7 wt%. The figure also includes the result for the nanocomposite film with 0.5 wt% LFGO loading. The OTR of GO/PLA nanocomposite films decreased with increasing GO content. As expected, the presence of graphene nanosheet with high aspect ratio in the nanocomposites effectively retarded the progress of oxygen molecules through the PLA matrix, resulting in a substantial decrease in OTR value. When incorporated with 0.5 wt% and 0.7 wt% GO, the oxygen barrier properties of resultant nanocomposite films were enhanced by 22% and 54%, respectively, relative to neat PLA film with measured OTR value of 572.7 cc $m^{-2}$ $day^{-1}$ $atm^{-1}$. In the case of 0.5 wt% LFGO-incorporated nanocomposite film, however, the OTR was decreased by only 5% from 572.7 to 542.0 cc $m^{-2}$ $day^{-1}$ $atm^{-1}$, indicating insignificant contribution of LFGO incorporation to the improvement in barrier performance. The GO nanosheets with larger amount of oxygen-containing functional groups were found to yield more prominent improvement in barrier performance for the nanocomposite film, relative to LFGO, in spite of their size reduction caused by severe oxidation and exfoliation process [17]. Accordingly, it is believed that highly functionalized graphene nanosheets can give rise to better compatibility with hydrophilic PLA resin, which is responsible for highly exfoliated nanostructured morphology, ultimately resulting in effective suppression of gas molecule permeation through the graphene-based nanocomposite film.

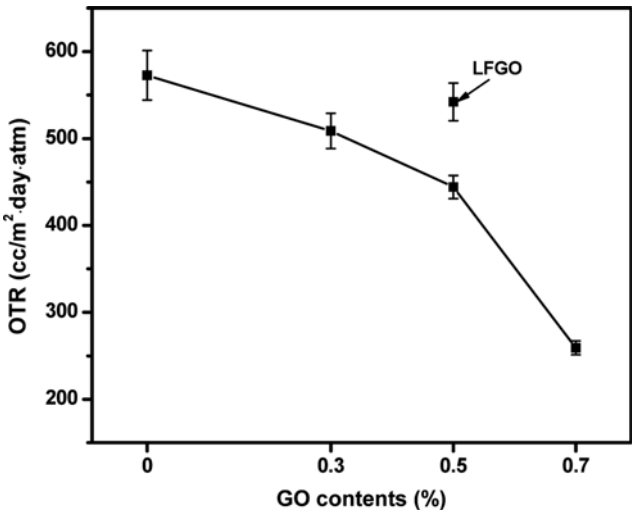


**Fig. 8. Oxygen transmission rate of GO/PLA films with various GO loading (0 to 0.7 wt%) and LFGO/PLA film with 0.5 wt% LFGO.**

## CONCLUSIONS

An enhancement in the physical and gas barrier properties of the biodegradable PLA film was achieved by incorporating small amounts of graphene oxide nanosheets (0.3 wt% to 0.7 wt%) via

solution blending method. XRD and TEM results showed that highly functionalized graphene oxide (GO) gave rise to more intercalated and exfoliated morphology as well as better dispersion in the hydrophilic PLA matrix, compared to low-functionalized graphene oxide (LFGO). Thermal properties such as $T_g$ and $\chi_c$, and mechanical properties of tensile strength and modulus were remarkably improved with increasing of GO loading, and more pronounced reinforcing effect was found in the case of GO incorporation, relative to LFGO nanofillers. On the other hand, only LFGO caused an improvement of the thermal stability in terms of TGA, because of a higher tendency of pyrolysis of GO containing larger amount of unstable functional groups. In addition, the incorporation of GO up to 0.7 wt% was revealed to yield the PLA-based nanocomposite films retaining fairly good transparency with light transmittance over 80%, as well as improved oxygen barrier performance, suggesting that GO would be more favorable for the achievement of high performance PLA-based nanocomposite film, compared to LFGO.

## ACKNOWLEDGEMENT

This work was supported by Kyonggi University Research Grant 2013.

## REFERENCES

1. K. Yang, X. Wang and Y. Wang, *J. Ind. Eng. Chem.*, **13**, 485 (2007).
2. N. Lilichenko, R. D. Maksimov, J. Zicans, R. M. Meri and E. Plume, *Mech. Compos. Mater.*, **44**, 45 (2008).
3. W. Amass, A. Amass and B. Tighe, *Polym. Int.*, **47**, 89 (1998).
4. J. Y. Nam, S. S. Ray and M. Okamoto, *Macromolecules*, **36**, 7126 (2003).
5. L. Lin, H. Liu and N. Yu, *J. Appl. Polym. Sci.*, **106**, 260 (2007).
6. S. Singh and S. S. Ray, *J. Nanosci. Nanotechnol.*, **7**, 2596 (2007).
7. J. Chang, Y. U. An and G. S. Sur, *J. Polym. Sci.:Part B: Polymer Physics*, **41**, 94 (2002).
8. V. Krikorian and D. J. Pochan, *Chem. Mater.*, **15**, 4317 (2003).
9. G. Bang and S. W. Kim, *J. Ind. Eng. Chem.*, **18**, 1063 (2012).
10. M. Iotti, P. Fabbri, M. Messori, F. Pilati and P. Fava, *J. Polym. Environ.*, **17**, 10 (2009).
11. H. Kim, A. A. Abdala and C. W. Mascosko, *Macromolecules*, **43**, 6515 (2010).
12. Y. F. Zhao, M. Xiao, S. J. Wang, X. C. Ge and Y. Z. Meng, *Compos. Sci. Technol.*, **67**, 2528 (2007).
13. Y. Lee, D. Kim, J. Seo, H. Han and S. B. Khan, *Polym. Int.*, **9**, 1386 (2013).
14. H. Huang, P. Ren, J. Chen, W. Zhang, X. Ji and Z. Li, *J. Membr. Sci.*, **409**, 156 (2012).
15. J. Wang, C. Xu, H. Hu, L. Wan, R. Chen, H. Zheng, F. Liu, M. Zhang, X. Shang and X. Wang, *J. Nanopart. Res.*, **13**, 869 (2011).
16. I. Tseng, Y. liao, J. Chiang and M. Tsai, *Mater. Chem. Phys.*, **136**, 247 (2012).
17. H. Kim, Y. Miura and C. W. Mascosko, *Chem. Mater.*, **22**, 3441 (2010).
18. J. Yang, L. Bai, G. Feng, X. Yang, M. Lv, C. Zhang, H. Hu and X. Wang, *Ind. Eng. Chem. Res.*, **52**, 16745 (2013).
19. A. M. Pinto, J. Cabral, D. A. Pacheco Tanaka, A. M. Mendes and F. D. Magalhaes, *Polym. Int.*, **62**, 33 (2013).
20. H. Wang and Z. Qiu, *Thermochim. Acta*, **527**, 40 (2012).
21. H. Wang and Z. Qiu, *Thermochim. Acta*, **526**, 229 (2011).
22. J. Z. Xu, T. Chen, C. L. Yang, Z. M. Li, Y. M. Mao, B. Q. Zeng and B. S. Hsiao, *Macromolecules*, **43**, 5000 (2010).
23. W. S. Hummers and R. E. Offman, *J. Am. Chem. Soc.*, **80**, 1339 (1958).
24. S. W. Kim and H. M. Choi, *High Perform. Polym.*, In Press DOI:10.1177/ 0954008314557051.
25. X. Zhao, Q. Zhang and D. Chen, *Macromolecules*, **43**, 2357 (2010).
26. S. Pei and H. M. Cheng, *Carbon*, **50**, 3210 (2012).
27. D. Zhou, Q. Y. Cheng and B. H. Han, *Carbon*, **49**, 3920 (2011).
28. W. S. Chow and S. K. Lok, *J. Therm. Anal. Cal.*, **95**, 627 (2009).
29. S. W. Kim, *Korean J. Chem. Eng.*, **28**, 298 (2011).
30. C. Chan and I. Chu, *Polymer*, **42**, 6089 (2001).
31. B. Finnigan, D. Martin, P. Halley, R. Truss and K. Campbell, *Polymer*, **45**, 2249 (2004).
32. X. Shi and Z. Gan, *Eur. Polym. J.*, **43**, 4852 (2007).
33. D. Wang, J. Yu, J. Zhang, J. He and J. Zhang, *Compos. Sci. Technol.*, **85**, 83 (2013).
34. J. Bian, H. L. Lin, F. X. He, L. Wang, X. W. Wei, I. Chang and E. Sancaktar, *Eur. Polym. J.*, **49**, 1406 (2013).
35. S. W. Kim and S. H. Cha, *J. Appl. Polym. Sci.*, **131**, 40289 (2014).